VEGF-B promotes cancer metastasis through a VEGF-A–independent mechanism and serves as a marker of poor prognosis for cancer patients

Xiaojuan Yang[a,b], Yin Zhang[a], Kayoko Hosaka[a], Patrik Andersson[a], Jian Wang[a], Fredrik Tholander[c], Ziquan Cao[d], Hiromasa Morikawa[e], Jesper Tegnér[e], Yunlong Yang[a], Hideki Iwamoto[a], Sharon Lim[a], and Yihai Cao[a,d,f,g,1]

[a]Department of Microbiology, Tumor and Cell Biology, Karolinska Institute, 171 77 Stockholm, Sweden; [b]Laboratory of Oral Biomedical Science and Translational Medicine, School of Stomatology, Tongji University, Shanghai 200072, Republic of China; [c]Department of Medical Biochemistry and Biophysics, Karolinska Institute, 171 77 Stockholm, Sweden; [d]Department of Medicine and Health Sciences, Linköping University, 581 83 Linköping, Sweden; [e]Unit of Computational Medicine, Department of Medicine, Center for Molecular Medicine, Karolinska Institute, 171 76 Stockholm, Sweden; [f]Department of Cardiovascular Sciences, University of Leicester, Leicester LE3 9QP, United Kingdom; and [g]National Institute for Health Research Leicester Cardiovascular Biomedical Research Unit, Glenfield Hospital, Leicester LE3 9QP, United Kingdom

Edited by Robert Langer, Massachusetts Institute of Technology, Cambridge, MA, and approved May 1, 2015 (received for review February 20, 2015)

The biological functions of VEGF-B in cancer progression remain poorly understood. Here, we report that VEGF-B promotes cancer metastasis through the remodeling of tumor microvasculature. Knockdown of VEGF-B in tumors resulted in increased perivascular cell coverage and impaired pulmonary metastasis of human melanomas. In contrast, the gain of VEGF-B function in tumors led to pseudonormalized tumor vasculatures that were highly leaky and poorly perfused. Tumors expressing high levels of VEGF-B were more metastatic, although primary tumor growth was largely impaired. Similarly, VEGF-B in a VEGF-A–null tumor resulted in attenuated primary tumor growth but substantial pulmonary metastases. VEGF-B also led to highly metastatic phenotypes in *Vegfr1 tk*$^{-/-}$ mice and mice treated with anti–VEGF-A. These data indicate that VEGF-B promotes cancer metastasis through a VEGF-A–independent mechanism. High expression levels of VEGF-B in two large-cohort studies of human patients with lung squamous cell carcinoma and melanoma correlated with poor survival. Taken together, our findings demonstrate that VEGF-B is a vascular remodeling factor promoting cancer metastasis and that targeting VEGF-B may be an important therapeutic approach for cancer metastasis.

VEGF-B | metastasis | VEGFR1 | VEGF-A | angiogenesis

Although genetic alterations of malignant cells govern the intrinsic features of invasiveness, host-derived cellular and molecular components may play predominant roles in cancer invasion and metastasis (1). For example, the tumor vasculature is essential for tumor growth and metastasis (2), and blocking tumor angiogenesis has been used successfully for treatment of animal and human cancers (3–5). Similarly, targeting other nonvascular host components, including inflammatory cells and stromal cells, also provides effective therapeutic options for treatment of cancer (6). Hematogenous metastasis is a complex process that involves intimate interactions between malignant cells and various host cells. At the primary tumor site, tumor cells must intravasate through the vessel wall into the circulation, and intravasation requires cooperative and coordinated interactions between tumor cells, perivascular cells such as pericytes, endothelial cells, and possibly inflammatory cells (7–9). In addition to their physical interactions, tumor cells and host cells produce various signaling molecules that modulate cell morphology, migration, proliferation, production of proteases, and adhesion molecules. Consequently, the vascular endothelium within and surrounding primary tumors undergoes structural changes that permit tumor cell invasion. After arriving at distal organs, tumor cells need to extravasate from the circulation. Again, circulating tumor cells interact closely with endothelial cells and perivascular cells to manipulate vascular structures for extravasation (10). The subsequent formation of metastatic niches and regrowth of metastatic nodules to clinically detectable masses are dependent on angiogenesis and vascular remodeling.

Tumors often express angiogenic factors at high levels to induce neovascularization (11). Multiple growth factors/cytokines and their signaling receptors often coexist in the same tumor microenvironment and collectively modulate tumor growth, invasiveness and metastasis (12). Among all known angiogenic factors, vascular endothelial growth factor A (VEGF-A), which modulates angiogenesis, vascular permeability, vessel survival, and vascular remodeling, is probably the best characterized (13, 14). Although VEGF-A binds to VEGF receptor 1 (VEGFR1) and VEGFR2, two tyrosine kinase receptors, it is believed that VEGFR2 mediates most of these VEGF-A–triggered vascular functions (15). Unlike VEGF-A, VEGF-B binds only to VEGFR1, which also is considered a decoy receptor that transduces negative signals for angiogenesis (16, 17). Despite its early discovery, the biological functions, and especially the vascular functions, of VEGF-B remain an enigma (18, 19). Initially, VEGF-B was shown to stimulate endothelial cell activity and angiogenesis (18). However, later studies do not support these claims, and opposing results that VEGF-B inhibits tumor angiogenesis have been reported (20, 21). The roles of VEGF-B in tumor invasion and metastasis have not been studied.

In this work, we report, for the first time to our knowledge, the crucial role of VEGF-B in modulating the vascular remodeling

Significance

Cancer metastasis is responsible for a majority of the mortality in cancer patients and involves complex interactions, modulated by various factors and cytokines, between malignant and host cells. Vascular structures in solid tumors are crucial for cancer cell intravasation into the circulation. Our present work shows that VEGF-B produced by tumor cells significantly remodels tumor microvasculature, leading to leaky vascular networks that are highly permissive for tumor cell invasion. VEGF-B–promoted cancer metastasis occurs through a VEGF-A–independent mechanism. Thus, inhibition of VEGF-B should be considered an independent approach for the development of new drugs for the treatment of cancer invasion and metastasis. VEGF-B also may be considered as an independent prognostic marker for cancer metastasis.

Author contributions: Y.C. designed research; X.Y., Y.Z., K.H., P.A., J.W., Z.C., Y.Y., H.I., and S.L. performed research; F.T., H.M., and J.T. contributed new reagents/analytic tools; X.Y., Y.Z., H.M., J.T., and Y.C. analyzed data; and Y.C. wrote the paper.

The authors declare no conflict of interest.

This article is a PNAS Direct Submission.

[1]To whom correspondence should be addressed. Email: yihai.cao@ki.se.

This article contains supporting information online at www.pnas.org/lookup/suppl/doi:10.1073/pnas.1503500112/-/DCSupplemental.

that facilitates tumor metastasis in human and mouse tumor models. Surprisingly, VEGF-B expression is reversely correlated with primary tumor growth, demonstrating that it negatively regulates tumor angiogenesis. Despite retarded growth rates of primary tumors, VEGF-B markedly promotes metastasis. Thus, primary tumor growth and metastasis are separate events, and the latter process is dependent on vascular alterations that become permissive for tumor invasion. Our present work provides compelling experimental evidence that VEGF-B is a metastatic factor and that targeting VEGF-B may be an important approach for the treatment of cancer invasion and metastasis.

Results

Loss of VEGF-B Function Improves Tumor Angiogenesis, Vascular Remodeling, Inflammation, and Hypoxia. To investigate the biological functions of VEGF-B in the tumor microenvironment and to relate our study to clinical relevance, we screened 28 human tumor cell lines for their expression of VEGF-B. These human tumor cell lines included melanoma, ovarian cancer, breast cancer, renal cell carcinoma, colorectal cancer, nonsmall cell lung carcinoma, retinoblastoma, glioblastoma, neuroblastoma, prostate cancer, cervical cancer, and epidermoid cancer (Table S1). First, we noticed that *VEGFB* expression was universally present in all tumor cell lines. Moreover, *VEGFB* mRNA expression varied widely in these cell lines, with a more than 30-fold difference between the cell line with the highest expression, UACC-257 melanoma, and that with the lowest expression, A431 epidermoid cancer (Table S1).

For further detailed analysis, we focused on the MDA-MB-435 melanoma cell line that expressed a relatively high level of *VEGFB* mRNA (Table S1). We took a loss-of-function approach by knocking down *VEGFB* using the specific shRNA. This knockdown approach effectively reduced *VEGFB* mRNA and protein expression levels in MDA-MB-435 melanoma cells. In

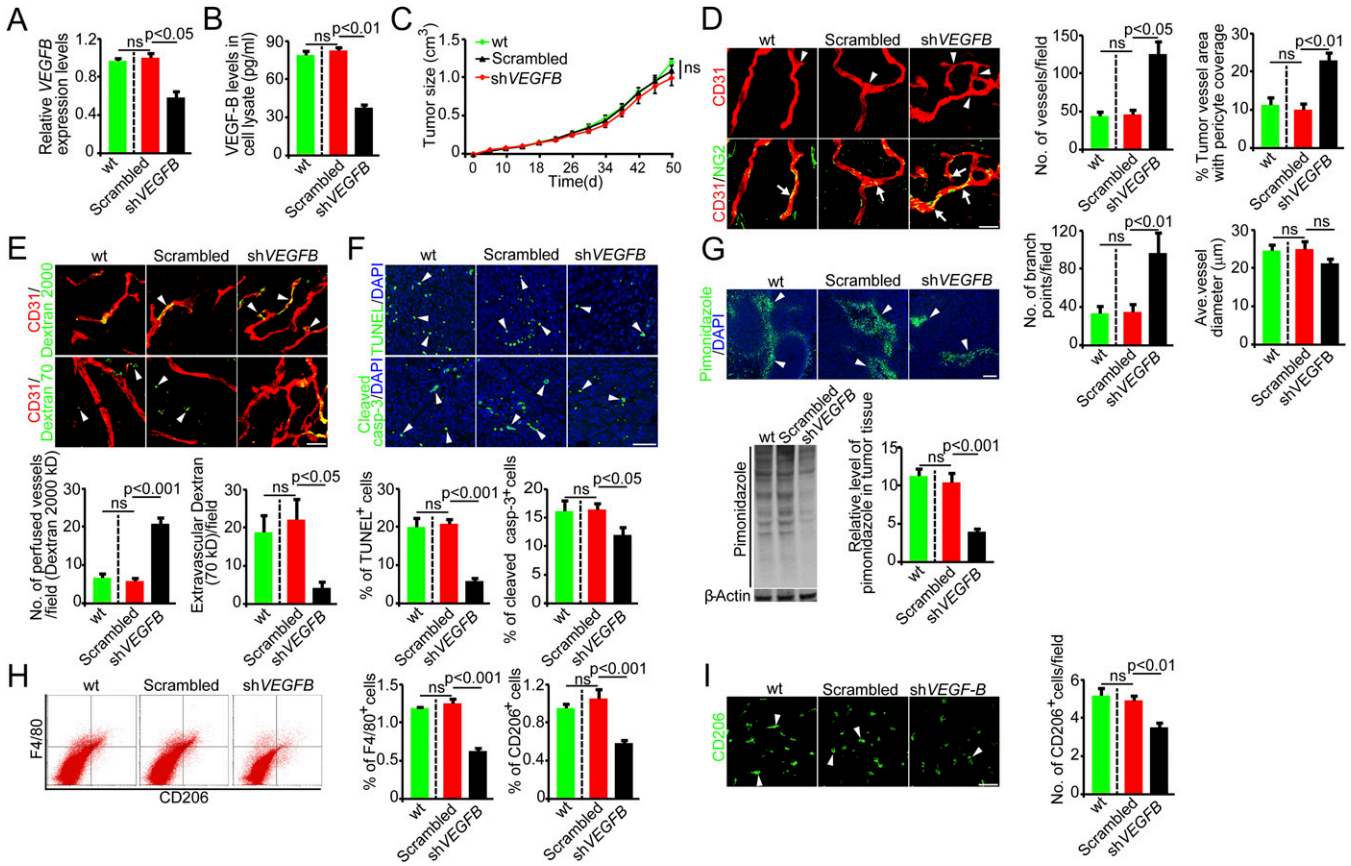

Fig. 1. Knockdown of VEGF-B induces vascular and microenvironmental changes in human melanomas. (*A*) VEGF-B knockdown in human MDA-MB-435 melanoma cells decreased *VEGFB* mRNA expression ($n = 3$ samples per group). (*B*) VEGF-B knockdown in human MDA-MB-435 melanoma cells decreases VEGF-B protein expression ($n = 3$ samples per group). (*C*) Tumor growth curves of WT, scrambled-shRNA-, and *VEGFB*-shRNA-MDA-MB-435 melanomas ($n = 20$ mice per group). (*D*, *Left*) Tumor vasculature of WT, scrambled-shRNA-, and *VEGFB*-shRNA-MDA-MB-435 melanomas. Arrowheads point to branch points, and arrows indicate pericyte coverage. (Scale bar, 50 μm.) (*Right*) Vessel numbers, pericyte coverage, branch points, and diameters of tumor vessels were quantified ($n = 24$ random fields per group). (*E*, *Upper*) Blood perfusion (2,000-kDa dextran) and vascular permeability (70-kDa dextran) of WT, scrambled-shRNA-, and *VEGFB*-shRNA-MDA-MB-435 melanomas. Arrowheads indicate perfused or leaked dextran signals. (Scale bar, 50 μm.) (*Lower*) Bar charts show the quantification of blood perfusion and leakiness ($n = 24$ random fields per group). (*F*, *Upper*) Measurement of cellular apoptosis by TUNEL and cleaved caspase-3 in WT, scrambled-shRNA-, and *VEGFB*-shRNA-transfected MDA-MB-435 melanomas. Arrowheads indicate apoptotic cells. (Scale bar, 50 μm.) (*Lower*) Quantification data are presented as the percentage of apoptotic cells versus total $DAPI^+$ cells ($n = 24$ random fields per group). (*G*) Measurement of tissue hypoxia in WT, scrambled-shRNA-, and *VEGFB*-shRNA-MDA-MB-435 melanomas. Immunofluorescent staining (*Upper*) and Western blotting (*Lower Left*) of the hypoxia probe pimonidazole. Arrowheads indicate pimonidazole-positive signals. (Scale bar, 100 μm.) (*Lower Right*) The bar chart shows the quantification of the pimonidazole signal ($n = 4$ samples per group). (*H*, *Left*) FACS measurement of $F4/80^+$ and $CD206^+$ macrophages in WT, scrambled-shRNA-, and *VEGFB*-shRNA-transfected MDA-MB-435 melanomas. (*Right*) Quantification is presented as the percentage of positive signals versus the total gated events ($n = 12$ samples per group). (*I*) Immunohistochemical analysis of $CD206^+$ macrophages in WT, scrambled-shRNA-, and *VEGFB*-shRNA-MDA-MB-435 melanomas ($n = 24$ fields per group). Arrowheads indicate $CD206^+$ macrophages. (Scale bar, 50 μm.) All error bars represent SEM. All *P* values were analyzed according to Student's *t* test. ns, not significant.

contrast, a scrambled control shRNA had no effect on *VEGFB* mRNA and protein expression (Fig. 1 *A* and *B*). Despite the reduced VEGF-B expression level, implantation of *VEGFB*-shRNA-MDA-MB-435 melanoma cells in syngeneic mice did not affect tumor growth (Fig. 1*C*), suggesting that in this cell line VEGF-B did not affect tumor growth rates in vivo. Similarly, no significant differences in tumor cell proliferation were observed between *VEGFB*-shRNA-MDA-MB-435 and scrambled-shRNA-MDA-MB-435 (Fig. S1*A*) tumors, indicating that VEGF-B expression had no effect on tumor cell proliferation per se. However, immunohistochemical examination of tumor microvessels revealed a marked increased of tumor vessel density in *VEGFB*-shRNA-MDA-MB-435 tumors compared with those in nontransfected WT and scrambled-shRNA-MDA-MB-435 tumors (Fig. 1*D*). These findings indicate that VEGF-B negatively regulates tumor angiogenesis. Interestingly, *VEGFB*-shRNA-MDA-MB-435 tumor vessels also contained a relatively higher density of $NG2^+$ pericytes, which remained associated with tumor microvessels (Fig. 1*D*). Another important finding was that tumor vessels underwent marked remodeling that switched from a normalized phenotype with few branches to a disorganized network with more branch points (Fig. 1*D*).

To relate VEGF-B–induced vascular remodeling to functional changes, we measured blood perfusion and the leakiness of tumor vessels. Notably, knockdown of VEGF-B in tumor cells led to a marked increase in blood perfusion (Fig. 1*E*). Conversely, vascular leakage of 70-kDa dextran was decreased significantly in *VEGFB*-shRNA-MDA-MB-435 tumors compared with WT and scrambled-shRNA tumors (Fig. 1*E*). Consistent with the improved blood perfusion and decreased leakiness, *VEGFB*-shRNA-MDA-MB-435 tumors showed improved tissue hypoxia (Fig. 1*G*), and this improvement in hypoxia led to significant decreases in cellular apoptosis (Fig. 1*F*). Intriguingly, $CD206^+$ and $F4/80^+$ tumor-associated macrophages (TAMs) were decreased significantly in *VEGFB*-shRNA-MDA-MB-435 tumors relative to WT and scrambled-shRNA tumors (Fig. 1 *H* and *I*). Taken together, these data demonstrate that VEGF-B–induced vascular remodeling has a significant impact, altering the tumor microenvironment.

Gain of VEGF-B Function Inhibits Angiogenesis and Blood Perfusion but Increases Vascular Leakage, Hypoxia, and Inflammation in Human and Mouse Tumors. We next performed gain-of-function experiments by knocking in VEGF-B in the human UACC-62 melanoma cell line that expresses a relatively low level of *VEGFB* (Table S1).

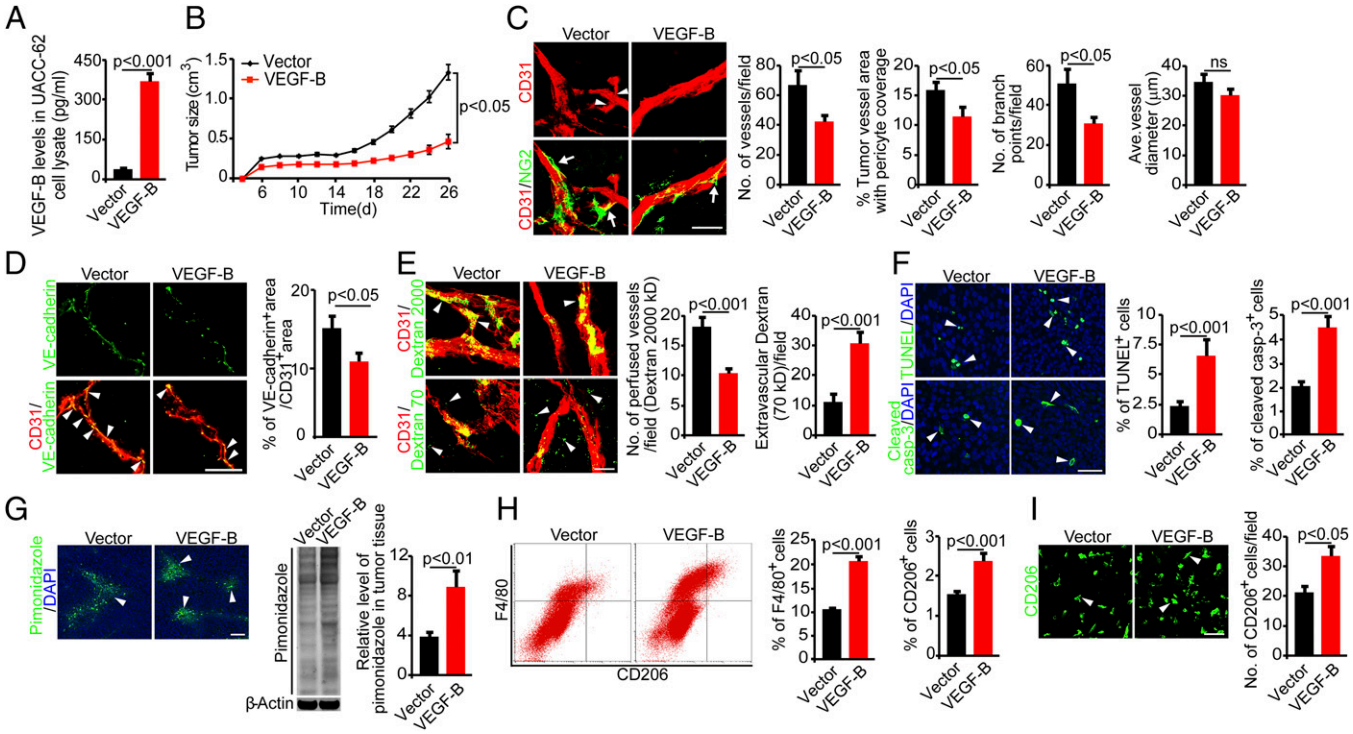

Fig. 2. Gain of VEGF-B function inhibits tumor growth by altering angiogenesis and vascular functions in human tumors. (*A*) Expression levels of VEGF-B protein in vector- and VEGF-B-UACC-62 tumor cells ($n = 3$ samples per group). (*B*) Tumor growth curves of vector- and VEGF-B-UACC-62 melanomas ($n = 20$ mice per group). (*C*, *Left*) Tumor vasculature of vector- and VEGF-B-UACC-62 melanomas. Arrowheads indicate branch points, and arrows indicate pericyte coverage. (Scale bar, 50 μm.) (*Right*) Vessel numbers, pericyte coverage, branch points, and diameters of tumor vessels were quantified ($n = 24$ random fields per group). (*D*, *Left*) VE-cadherin (green) and CD31 (red) double immunostaining of vector- and VEGF-B-UACC-62 melanomas. Arrowheads indicate double immunopositive signals (yellow). (Scale bar, 50 μm.) (*Right*) Quantification of VE-cadherin–positive signals in tumor vessels ($n = 10$–13 random fields per group). (*E*, *Left*) Blood perfusion (2,000-kDa dextran) and vascular permeability (70-kDa dextran) of vector- and VEGF-B-UACC-62 melanomas. Arrowheads indicate perfused or leaked dextran signals. (Scale bar, 50 μm.) (*Right*) Quantification of blood perfusion and leakiness ($n = 24$ random fields per group). (*F*, *Left*) Measurement of cellular apoptosis by TUNEL and cleaved caspase-3 in vector- and VEGF-B-UACC-62 melanomas. Arrowheads indicate apoptotic cells. (Scale bar, 50 μm.) (*Right*) Quantification data are presented as the percentage of apoptotic cells versus total $DAPI^+$ cells ($n = 24$ random fields per group). (*G*) Measurement of tissue hypoxia of vector- and VEGF-B-UACC-62 melanomas. (*Left*) Immunofluorescent staining of the hypoxia probe pimonidazole. Arrowheads indicate pimonidazole-positive signals. (Scale bar, 100 μm.) (*Center*) Western blotting of the hypoxia probe pimonidazole. (*Right*) Quantification is presented as the relative level of pimonidazole in tumor tissue. ($n = 4$ samples per group) (*H*, *Left*) FACS measurement of $F4/80^+$ and $CD206^+$ macrophages in vector- and VEGF-B-UACC-62 melanomas. (*Right*) Quantification is presented as the percentage of positive signals versus the total gated events ($n = 12$ samples per group). (*I*, *Left*) Immunohistochemical analysis of $CD206^+$ macrophages of vector- and VEGF-B-UACC-62 melanomas ($n = 24$ fields per group). Arrowheads indicate $CD206^+$ macrophages. (Scale bar, 50 μm.) (*Right*) Quantification is presented as the number of $CD206^+$ cells per field. All error bars represent SEM. All *P* values were analyzed according to Student's *t* test. ns, not significant.

Transfection of UACC-62 tumor cells with the *VEGF-B* gene resulted in approximately sevenfold increases in VEGF-B protein expression relative to the vector-transfected tumor cells (Fig. 2*A*). Surprisingly, enforced expression of VEGF-B in UACC-62 tumors led to significantly suppressed primary tumor growth compared with vector control tumors (Fig. 2*B*). These data indicate that VEGF-B negatively regulates primary tumor growth. Consistent with the inhibition of primary tumor growth, the microvessel density of VEGF-B-UACC-62 melanoma tumors also was reduced significantly (Fig. 2*C*), suggesting that VEGF-B negatively modulates tumor angiogenesis. Further, tumor vessels in VEGF-B-UACC-62 tumors manifested as a normalized phenotype that lacked excessive sprouting and branches, although the diameters of tumor microvessels were not altered (Fig. 2*C* and Fig. S2*A*). Despite vascular normalization by VEGF-B in these tumors, these pseudonormalized tumor vessels were poorly covered with pericytes (Fig. 2*C*). Additionally, VE-cadherin was decreased significantly in the vasculature of VEGF-B–expressing tumors as compared with control tumors (Fig. 2*D*). These findings indicate that endothelial cell junctions of vessels in VEGF-B tumors were significantly impaired, supporting the notion that VEGF-B–expressing tumor vessels were more vulnerable to tumor cell intravasation. In contrast, collagen IV and fibronectin, two main basement membrane components of blood vessels, were not altered in VEGF-B tumors as compared with control tumors (Fig. S2*B*). Consistently, VEGF-B–induced pseudonormalized tumor vessels were highly leaky and poorly perfused compared with those in vector-UACC-62 tumors (Fig. 2*E*). These gain-of-function experiments validate our data obtained from the loss-of-function experimental settings, which collectively showed that VEGF-B is a negative regulator of tumor angiogenesis and tumor growth.

As a consequence of heavy leakage and poor perfusion of tumor vessels, VEGF-B-UACC-62 tumors exhibited a higher degree of tissue hypoxia than seen in vector-UACC-62 tumors (Fig. 2*G*). These findings were validated further by a quantitative immunoblotting analysis (Fig. 2*G*). A marked increase in cellular apoptosis also was detected in hypoxic VEGF-B-UACC-62 tumors as compared with control tumors (Fig. 2*F*). Moreover, the percentage of inflammatory F4/80$^+$ macrophages was increased significantly in VEGF-B-UACC-62 tumors (Fig. 2*H*). Notably, the CD206$^+$ M2-like TAMs also were increased dramatically (Fig. 2*I*). These findings show that the gain of VEGF-B function in an intrinsically low VEGF-B tumor inhibits tumor angiogenesis and remodels tumor vasculature toward a leaky and poor-perfusion phenotype that increases tissue hypoxia.

To validate our findings further, we chose a mouse fibrosarcoma (T241 fibrosarcoma) that expressed barely detectable VEGF-B protein (Fig. S3*A*). As in human tumors, overexpression of VEGF-B significantly inhibited primary tumor growth (Fig. S3*B*). Again, tumor-derived VEGF-B inhibited tumor angiogenesis considerably, leading to a normalized phenotype with very few sprouting braches compared with the vector-T241 tumors (Fig. S3*C*). Paradoxically, these VEGF-B–induced pseudonormalized tumor vasculatures were poorly coated with NG2$^+$ pericytes compared with those in control tumor tissues (Fig. S3*C*). Consistent with the poor coverage of pericytes, VEGF-B tumor vasculature was highly leaky and showed increased extravasation of 70-kDa dextran molecules (Fig. S3*D*). In contrast, vascular perfusion in VEGF-B-T241 tumors was decreased significantly (Fig. S3*D*). The decreased blood perfusion in VEGF-B-T241 tumors might explain the anti-tumor growth effect of VEGF-B.

Similar to human tumors, VEGF-B-T241 tumors also exhibited increased tissue hypoxia, which was detected by immunohistochemistry and immunoblotting of pimonidazole-positive signals (Fig. S3*E*). The apoptotic rate also was higher in VEGF-B-T241 tumors than in control tumors (Fig. S3*F*). Apoptotic tumor cells were detected and quantified by TUNEL detection and cleaved caspase-3 staining. FACS analysis showed that the percentage of F4/80$^+$ TAMs was increased markedly (Fig. S3*G*). Interestingly, the CD206$^+$ M2-like subpopulation of macrophages was increased significantly in VEGF-B-T241 tumors (Fig. S3 *G* and *H*). All these findings obtained from mouse tumors validate our finding that VEGF-B negatively modulates tumor angiogenesis but markedly increases tumor hypoxia and inflammation.

VEGF-B Promotes Tumor Hematogenous Metastasis in Human and Mouse Tumor Models. Our findings from human and mouse tumor models described above suggest three independent mechanisms by which VEGF-B promotes tumor invasion and metastasis: (*i*) ablation of perivascular cells and increase of vascular leakiness; (*ii*) a high degree of tumor hypoxia; and (*iii*) an increase in TAMs, especially M2-like TAMs. Therefore we studied the invasive and metastatic features of VEGF-B in both gain-of-function and loss-of-function experimental settings. The number of circulating tumor cells (CTCs) was decreased significantly in mice bearing *VEGFB*-shRNA-MDA-MB-435 tumors as compared with mice bearing scrambled-shRNA-MDA-MB-435 tumors (Fig. 3*A*). Consistent with the reduction of CTCs, pulmonary metastatic human melanomas were reduced significantly in mice bearing *VEGFB*-shRNA-MDA-MB-435 tumors relative to mice bearing control tumors (Fig. 3*B*). The presence of pulmonary metastatic lesions was confirmed further by H&E histological analysis and immunohistological staining of fluorescent-labeled tumor cells (Fig. 3*B*).

Conversely, the gain of VEGF-B function in human UACC-62 melanoma (in which VEGF-B expression is intrinsically low) led to a considerably increased number of CTCs in tumor-bearing mice (Fig. 3*C*). Notably, CTCs were increased approximately fivefold in mice bearing VEGF-B-UACC-62 tumors as compared with mice bearing control tumors (Fig. 3*C*). Importantly, mice bearing VEGF-B-UACC-62 tumors carried significantly increased pulmonary metastases that were RFP$^+$ (Fig. 3*D*). As in human VEGF-B-UACC-62 tumors, higher VEGF-B expression in T241 tumors also resulted in a considerable increase in CTCs and lung metastasis compared with the control groups (Fig. 3 *E* and *F*). It should be emphasized that the magnitude of increases in lung metastasis by VEGF-B was considerably greater in the T241 fibrosarcoma model than in melanoma models (Fig. 3*F*), perhaps because of the low intrinsic basal level of VEGF-B in this tumor cell line. In summary, in both human and mouse tumor models we found convincing and compelling evidence that VEGF-B substantially promotes cancer metastasis.

VEGF-B Increases the Dissemination of Human and Mouse Tumor Cells in Zebrafish Models. VEGF-B–induced vascular and the tumor microenvironmental changes, including ablation of perivascular cells from microvessels and increases in vascular leakiness, inflammation, and hypoxia, suggested to us that VEGF-B–promoted cancer metastasis occurs at the initial step of the metastatic cascade, i.e., intravasation of tumor cells into the circulation. We recently have developed a zebrafish metastasis model that permits the investigation of tumor cell invasion at the single-cell level (22–24). Moreover, this zebrafish model allows direct visualization of the early events of cancer metastasis such as intravasation of tumor cells into the circulation in the living body. Given these advantages, we further studied the role of VEGF-B in cancer metastasis using this model. Implantation of 1,1-Dioctadecyl-3,3,3,3-tetramethylindocarbocyanine perchlorate (DiI)-labeled WT human MDA-MB-435 melanoma cells into the perivitelline space of zebrafish embryos produced broad dissemination and metastasis in the zebrafish body (Fig. S4 *A* and *B*). The relation between disseminated tumor cells and vasculature was investigated using the transgenic Fli1:EGFP zebrafish strain (25). A similar metastatic pattern also was found in zebrafish embryos implanted with scrambled-shRNA-MDA-MB-435 tumors (Fig. S4 *A* and *B*). In contrast, the number of metastatic cells was significantly

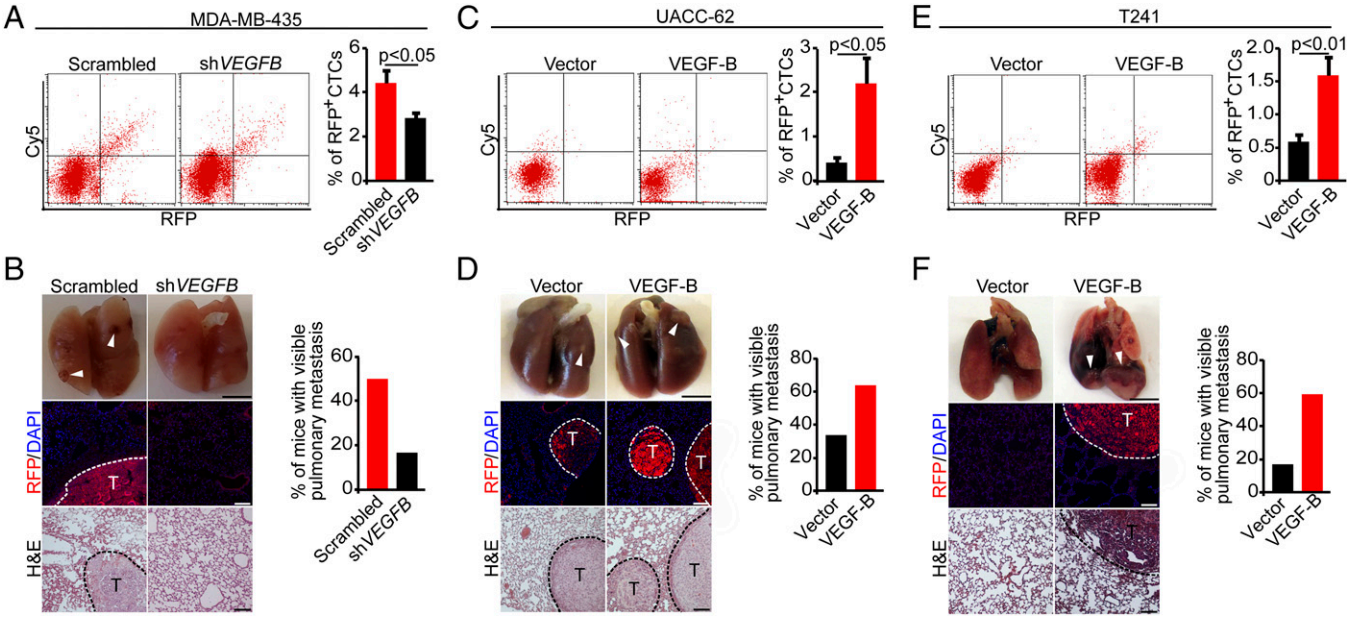

Fig. 3. Cancer metastasis in VEGF-B loss-of-function and gain-of-function tumor models. (*A*, *Left*) FACS analysis of CTCs in mice bearing scrambled-shRNA- and *VEGFB*-shRNA-MDA-MB-435 melanomas. (*Right*) Quantification of CTCs is presented as the percentage of positive signals versus the total gated events ($n = 12$ samples per group). (*B*, *Left*) Pulmonary metastasis in SCID mice bearing scrambled-shRNA- and *VEGFB*-shRNA-MDA-MB-435 melanomas. Arrowheads indicate metastatic nodules. Dashed lines encircle metastatic nodules. [Scale bars, 5 mm (*Top*); 100 μm (*Middle* and *Bottom*).] (*Right*) The bar chart shows the percentage of mice with visible lung metastases ($n = 12$ animals per group). (*C*, *Left*) FACS analysis of CTCs in mice bearing human vector- and VEGF-B-UACC-62 melanomas. (*Right*) Quantification of CTCs is presented as the percentage of positive signals versus the total gated events ($n = 11$–12 samples per group). (*D*, *Left*) Pulmonary metastasis in SCID mice bearing human vector- and VEGF-B-UACC-62 melanomas. Arrowheads indicate metastatic nodules. Dashed lines encircle metastatic nodules. [Scale bars, 5 mm (*Top*); 100 μm (*Middle* and *Bottom*).] (*Right*) The bar chart shows the percentage of mice with visible lung metastases ($n = 12$ animals per group). (*E*, *Left*) FACS analysis of CTCs in mice bearing mouse vector- and VEGF-B-T241 melanomas. (*Right*) Quantification of CTCs is presented as the percentage of positive signals versus the total gated events ($n = 12$ samples per group). (*F*, *Left*) Pulmonary metastasis in C57BL/6 mice bearing mouse vector- and VEGF-B-T241 tumors. Arrowheads indicate metastatic nodules. Dashed lines encircle metastatic nodules. [Scale bars, 5 mm (*Top*); 100 μm (*Middle* and *Bottom*).] (*Right*) The bar chart shows the percentage of mice with visible lung metastases ($n = 10$ animals per group). All error bars represent SEM. All *P* values were analyzed according to Student's *t* test.

lower in zebrafish embryos implanted with *VEGFB*-shRNA-MDA-MB-435 tumors than in zebrafish embryos implanted with control tumors (Fig. S4 *A* and *B*). These findings further support the notion that VEGF-B promotes cancer metastasis.

In contrast to the knockdown of VEGF-B in human melanoma, the gain of VEGF-B expression in UACC-62 tumors resulted in widespread cancer cells in zebrafish bodies. At day 4 after tumor cell implantation, VEGF-B-UACC-62 primary tumor cells had disappeared almost completely due to dissemination of tumor cells to various parts of the zebrafish body (Fig. S4 *C* and *D*). Likewise, the zebrafish bearing VEGF-B-T241 tumors exhibited a similar broad metastatic pattern (Fig. S4 *E* and *F*). Taken together, our findings in the zebrafish metastasis model indicate that VEGF-B is a potent prometastatic factor.

VEGF-B Promotes Metastasis Through a VEGF-A–Independent Mechanism. Previous studies showed that VEGF-B modulates VEGF-A–induced angiogenesis (20). To investigate the relation between VEGF-B and VEGF-A in tumor angiogenesis and metastasis, we used a VEGF-A–null tumor cell line (528ras) that was generated from *Vegfa*$^{-/-}$ mouse embryonic fibroblasts (26). We transfected the 528ras-VEGF-A–null tumor cells with *VEGFB* cDNA to express VEGF-B specifically at a high level in the absence of VEGF-A (Fig. 4*A*). VEGF-B-528ras tumors implanted in mice showed significantly delayed tumor growth compared with vector-528ras tumors (Fig. 4*B*), indicating that VEGF-B–inhibited tumor growth does not depend on the presence of VEGF-A in tumor cells. Surprisingly, microvessels in VEGF-B-528ras tumors showed more sprouts and branches than microvessels vessels in vector-528ras tumors (Fig. 4*C*). This effect of the VEGF-B on tumor vessels in VEGF-A–null tumors opposed that in VEGF-A^{+} tumors, suggesting that VEGF-B modulates vascular remodeling in collaboration with VEGF-A.

Along with the increase of vascular branches, the vascular coverage of perivascular cells was reduced significantly in VEGF-B-528ras tumors (Fig. 4*C*). Although blood perfusion per histological area remained similar in VEGF-B-528ras and vector-528ras tumors, tumor vessels in VEGF-B-528ras were highly leaky (Fig. 4*D*). Despite these vascular changes, tissue hypoxia did not differ significantly in VEGF-B-528ras and vector-528ras tumors (Fig. S5). However, the F4/80^{+} macrophages and the CD206^{+} M2-like macrophage subpopulation were increased significantly in VEGF-B-528ras tumors (Fig. 4*E*). Consistent with the increases in vascular tortuosity, the reduction of perivascular cell coverage, and increased vascular permeability, CTCs were increased approximately threefold in mice bearing VEGF-B-528ras tumors relative to mice bearing vector-528ras tumors (Fig. 4*F*). Consequently, the high number of CTCs in mice bearing VEGF-B-528ras tumors led to increased lung metastatic lesions that expressed RFP (Fig. 4*G*). These results show that VEGF-B promotes cancer metastasis through a mechanism that is independent of VEGF-A. Furthermore, a highly significant increase in the distant dissemination of VEGF-B-528ras tumor cells was found in the zebrafish model, whereas vector-528ras tumor cells were rarely seen in zebrafish trunk areas (Fig. 4*H*).

Anti–VEGF-A Treatment Did Not Block VEGF-B–Induced Cancer Metastasis. Genetic deletion of the *Vegfa* gene in tumor cells did not exclude the possibility that host cell-derived VEGF-A still might play a role in collaborating with VEGF-B for metastasis. To eliminate the host cell-derived VEGF-A from participating in VEGF-B–induced

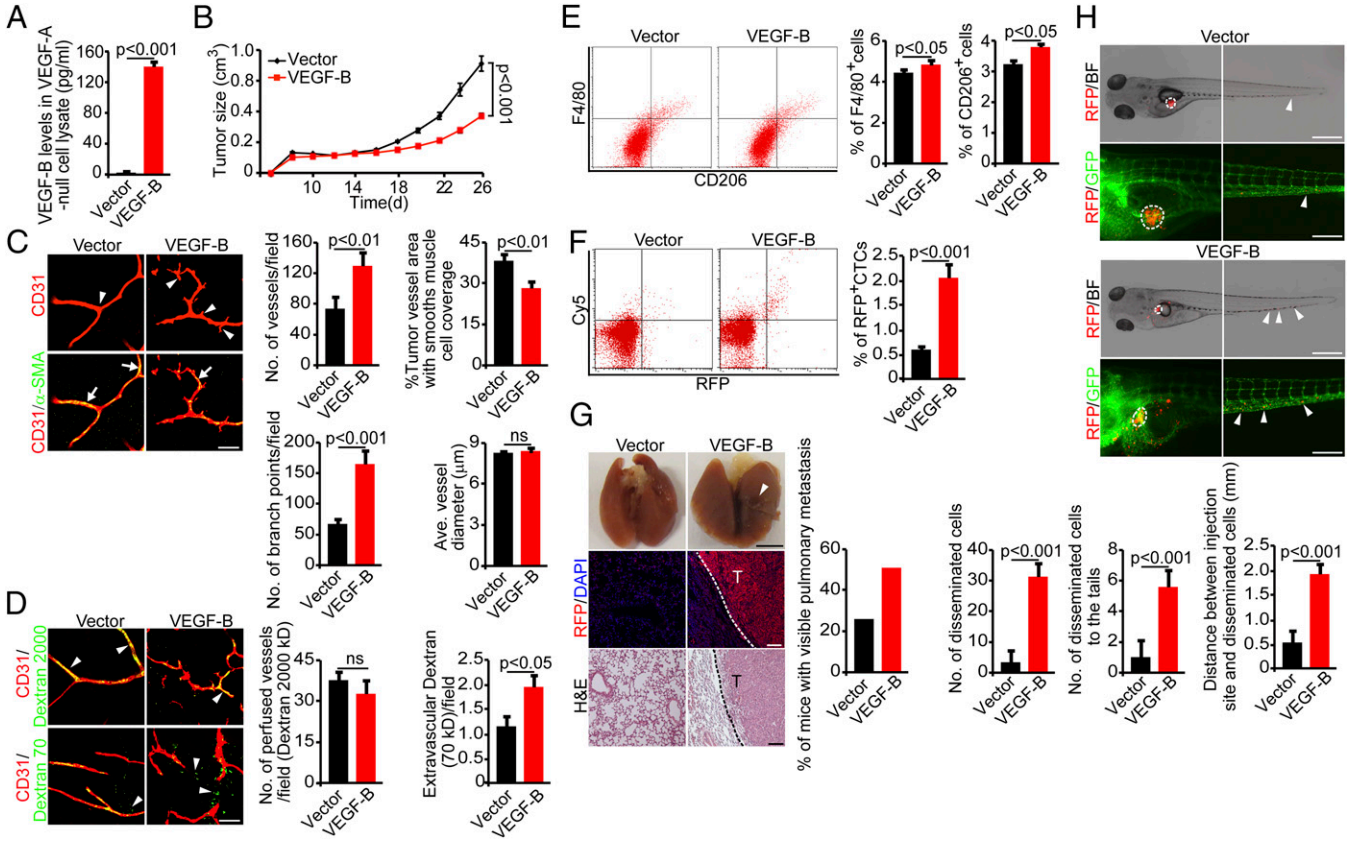

Fig. 4. Gain of VEGF-B function in VEGF-A–null tumors inhibits tumor growth by altering angiogenesis and vascular functions in mouse tumors. (*A*) Expression levels of VEGF-B protein in VEGF-A–null 528ras fibrosarcoma tumor cells. ($n = 3$ samples per group). (*B*) Tumor growth curves of vector- and VEGF-B-528ras fibrosarcoma tumors ($n = 20$ mice per group). (*C, Left*) Tumor vasculature of vector- and VEGF-B-528ras tumors. Arrowheads point to vascular branches, and arrows indicate perivascular cell coverage. (Scale bar, 50 μm.) (*Right*) Vessel numbers, coverage of perivascular cells, branch points, and diameters of tumor vessels were quantified ($n = 24$ random fields per group). (*D*, *Left*) Blood perfusion (2,000-kDa dextran) and vascular permeability (70-kDa dextran) of vector- and VEGF-B-528ras tumors. Arrowheads indicate perfused or leaked dextran signals. (Scale bar, 50 μm.) (*Right*) Quantification of blood perfusion and leakiness ($n = 24$ random fields per group). (*E*, *Left*) FACS measurement of F4/80$^+$ and CD206$^+$ macrophages of vector- and VEGF-B-528ras tumors. (*Right*) Quantification is presented as the percentage of positive signals versus the total gated events ($n = 12$ samples per group). (*F*, *Left*) FACS analysis of CTCs in mice bearing vector- and VEGF-B-528ras tumors. (*Right*) Quantification of CTCs is presented as the percentage of positive signals versus the total gated events ($n = 12$ samples per group). (*G*, *Left*) Pulmonary metastasis in SCID mice bearing vector- and VEGF-B-528ras tumors. Arrowheads indicate metastatic nodules. Dashed lines encircle metastatic nodules. [Scale bar, 5 mm (*Top*); 100 μm (*Middle* and *Bottom*).] (*Right*) The bar chart shows the percentage of mice with visible lung metastases ($n = 12$ animals per group). (*H*, *Top* and *Middle*) Dissemination of DiI-labeled mouse vector- (*Top*) and VEGF-528ras (*Middle*) tumor cells in zebrafish. Dashed lines encircle primary tumor sites. Arrowheads point to the disseminated tumor cells. [Scale bar, 500 μm (*Top*); 200 μm (*Middle*).] (*Bottom*) The bar charts show the quantification of disseminated tumor cells in the whole body of zebrafish embryos ($n = 10$ zebrafish embryos per group). All error bars represent SEM. All *P* values were analyzed according to Student's *t* test. BF, bright field; ns, not significant.

metastasis, we took a pharmacological approach to inhibit VEGF-A in mice bearing murine fibrosarcoma tumors. As expected, treatment of mice bearing vector-T241 tumors with an anti-mouse VEGF-A neutralizing antibody (VEGF-A blockade) (27–29) resulted in normalized vasculature (Fig. 5*A*). Surprisingly, under treatment with the VEGF-A blockade, a high VEGF-B level did not result in excessive vessel sprouts and branches as seen in VEGF-A–null VEGF-B-528ras tumors (Fig. 4*C*). These findings show that host VEGF-A in the VEGF-A–null 528ras tumor model was responsible for the excessive sprouting and branch formation of tumor vessels (Fig. 4*C*). Along with reduced vascular numbers, blood perfusion in the tumor treated with anti–VEGF-A was decreased further in VEGF-B-T241 tumors (Fig. 5*B*). Like the untreated tumors, VEGF-B-T241 tumors treated with anti–VEGF-A contained highly leaky vasculature relative to vector-T241 tumors treated with anti–VEGF-A (Fig. 5*B*).

Decreased blood perfusion and increased leakiness in VEGF-B-T241 tumors treated with anti–VEGF-A significantly elevated tumor hypoxia (Fig. 5*C*). Additionally, the CD206$^+$ macrophage subpopulation also was increased in the VEGF-B-T241 tumors treated with VEGF-A blockade relative to similarly treated vector-T241 tumors (Fig. 5*D*). CTC numbers in the VEGF-B-T241 tumors treated with anti–VEGF-A increased nearly sevenfold relative to vector-T241 tumors treated with anti–VEGF-A (Fig. 5*E*). Again, the increased CTC numbers correlated positively with increased lung metastasis in mice bearing VEGF-B-T241 tumors treated with anti–VEGF-A (Fig. 5*F*). These findings show that treatment with anti–VEGF-A did not block VEGF-B–induced cancer metastasis, thus supporting the notion that VEGF-B promotes cancer metastasis through a VEGF-A–independent mechanism.

VEGF-B Induces VEGFR1-Independent Cancer Metastasis. Because VEGFR1 is the key receptor for VEGF-B, we studied VEGFR1 involvement in cancer metastasis. To do so, we took a genetic approach, using *Vegfr1 tk*$^{-/-}$ mice that lacked functional tyrosine kinase activity of VEGFR1 (30). Implantation of VEGF-B-T241 tumors in *Vegfr1 tk*$^{-/-}$ mice produced a marked anti-tumor growth effect (Fig. 6*A*). Notably, the anti-tumor growth effect of VEGF-B in *Vegfr1 tk*$^{-/-}$ mice was similar to that in WT mice, and VEGF-B-T241 tumors in *Vegfr1 tk*$^{-/-}$ mice also showed marked reduction of vessel density, vascular branches, pericyte coverage, and blood

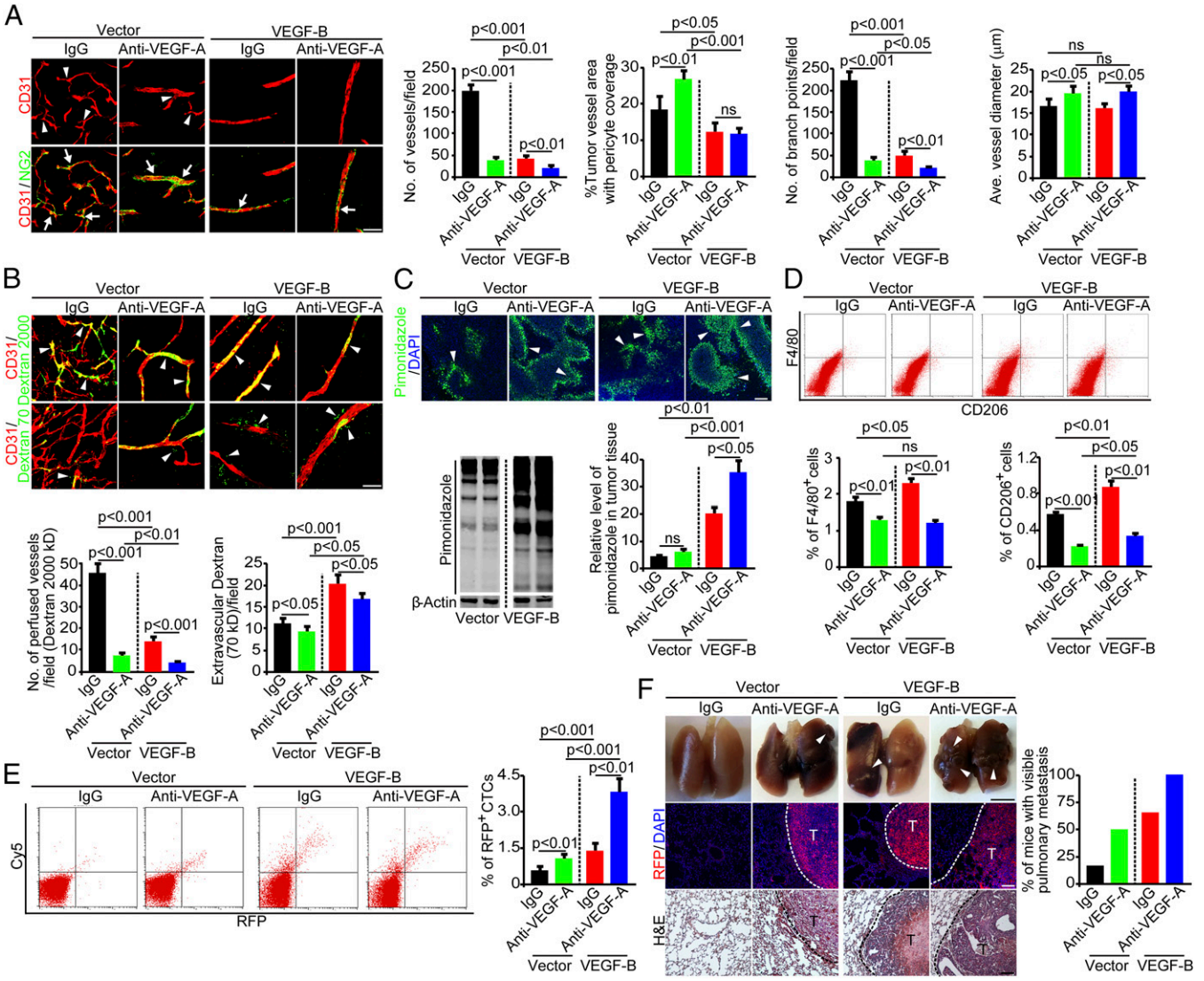

Fig. 5. VEGF-B induces anti–VEGF-A–independent metastasis. (*A*, *Left*) Tumor vasculature of control IgG-treated and anti–VEGF-A–treated vector- and VEGF-B-T241 tumors. Arrowheads point to vascular branches, and arrows indicate pericyte coverage. (Scale bar, 50 μm.) (*Right*) Vessel numbers, pericyte coverage, branch points, and diameters of tumor vessels were quantified ($n = 24$ random fields per group). (*B*, *Upper*) Blood perfusion (2,000-kDa dextran) and vascular permeability (70-kDa dextran) of control IgG-treated tumors and tumors treated with anti–VEGF-A. Arrowheads indicate perfused or leaked dextran signals. (Scale bar, 50 μm.) (*Lower*) Quantification of blood perfusion and leakiness ($n = 24$ random fields per group). (*C*) Measurement of tissue hypoxia in control IgG-treated tumors and tumors treated with anti–VEGF-A. (*Upper*) Immunofluorescent staining of the hypoxia probe pimonidazole. Arrowheads indicate pimonidazole-positive signals. (Scale bar, 100 μm.) (*Lower Left*) Western blotting of the hypoxia probe pimonidazole. (*Lower Right*) The bar chart shows the quantification of the pimonidazole signal ($n = 3$ samples per group). (*D*, *Upper*) FACS measurement of F4/80$^+$ and CD206$^+$ macrophages of control IgG-treated tumors and tumors treated with anti–VEGF-A. (*Lower*) Quantification is presented as the percentage of positive signals versus the total gated events ($n = 12$ samples per group). (*E*, *Left*) FACS analysis of CTCs in mice bearing control IgG-treated tumors and tumors treated with anti–VEGF-A. (*Right*) Quantification of CTCs is presented as the percentage of positive signals versus the total gated events ($n = 12$ samples per group). (*F*, *Left*) Pulmonary metastasis in mice bearing control IgG-treated tumors and tumors treated with anti–VEGF-A. Arrowheads indicate metastatic nodules. Dashed lines encircle metastatic nodules. [Scale bar, 5 mm (*Top*); 100 μm (*Middle* and *Bottom*).] (*Right*) The bar chart shows percentage of mice with visible lung metastases ($n = 11$–12 animals per group). All error bars represent SEM. All *P* values were analyzed according to Student's *t* test. ns, not significant.

perfusion (Fig. 6 *B* and *C*). In contrast, vascular leakage, tissue hypoxia, and infiltration of the total and M2-like macrophages were increased significantly (Fig. 6 *C*–*E*). Similar to tumor-bearing WT mice, *Vegfr1 tk*$^{-/-}$ mice bearing VEGF-B-T241 tumors showed markedly higher numbers of CTCs and more pulmonary metastasis than *Vegfr1 tk*$^{-/-}$ mice bearing vector-T241 tumors (Fig. 6 *F* and *G*). Collectively, these findings show that genetic deletion of the tyrosine kinase domain of VEGFR1 in mice did not completely prevent VEGF-B–induced cancer metastasis. Therefore, it is reasonable to speculate that VEGF-B promotes cancer metastasis through a VEGFR1-independent mechanism.

Reverse Correlation of VEGF-B Expression and Survival in Human Cancer Patients. Given its metastatic functions, we speculated that VEGF-B expression in tumor tissues would correlate reversely with survival in human cancer patients, because cancer metastasis is one of the main causes of mortality in these patients. We therefore analyzed the correlation of VEGF-B expression levels in human tumors with cancer patient survival in two cohort studies. Patients were divided into two groups according to the level of *VEGFB* mRNA expression in tumors. Patients in whom *VEGFB* expression levels were above the average were deemed the high-expression group, and those in whom *VEGFB* expression was below the

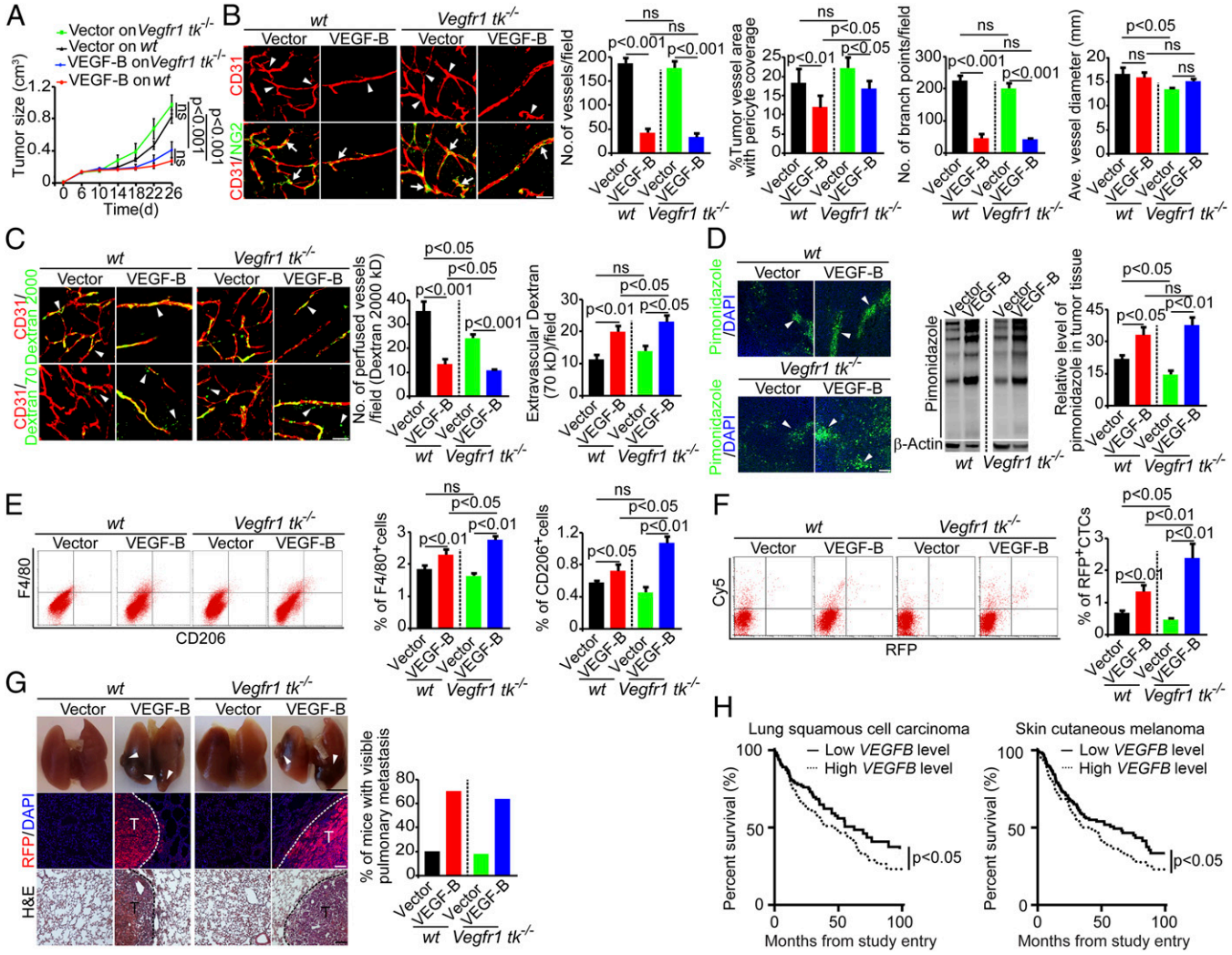

Fig. 6. VEGF-B induces metastasis in *Vegfr1 tk*$^{-/-}$ mice. (*A*) Tumor growth curves of vector- and VEGF-B-T241 tumors in WT and *Vegfr1 tk*$^{-/-}$ mice (n = 18–20 mice per group). (*B*, *Left*) Vasculature of vector- and VEGF-B-T241 tumors in WT and *Vegfr1 tk*$^{-/-}$ mice. Arrowheads point to vascular branches, and arrows indicate pericyte coverage. (Scale bar, 50 μm.) (*Right*) Vessel numbers, pericyte coverage, branch points, and diameters of tumor vessels were quantified (n = 24 random fields per group). (*C*, *Left*) Blood perfusion (2,000-kDa dextran) and vascular permeability (70-kDa dextran) of vector- and VEGF-B-T241 tumors in WT and *Vegfr1 tk*$^{-/-}$ mice. Arrowheads indicate perfused or leaked dextran signals. (Scale bar, 50 μm.) (*Right*) Quantification of blood perfusion and leakiness (n = 24 random fields per group). (*D*) Measurement of tissue hypoxia in vector- and VEGF-B-T241 tumors in WT and *Vegfr1 tk*$^{-/-}$ mice. (*Left*) Immunofluorescent staining of the hypoxia probe pimonidazole. Arrowheads indicate pimonidazole-positive signals. (Scale bar, 100 μm.) (*Center*) Western blotting of the hypoxia probe pimonidazole. (*Right*) The bar chart shows the quantification of pimonidazole signal (n = 3 samples per group). (*E*, *Left*) FACS measurement of F4/80$^+$ and CD206$^+$ macrophages of vector- and VEGF-B-T241 tumors in WT and *Vegfr1 tk*$^{-/-}$ mice. (*Right*) Quantification is presented as the percentage of positive signals versus the total gated events (n = 12 samples per group). (*F*, *Left*) FACS analysis of CTCs in WT and *Vegfr1 tk*$^{-/-}$ mice bearing vector- and VEGF-B-T241 tumors. (*Right*) Quantification of CTCs is presented as the percentage of positive signals versus the total gated events (n = 12 samples per group). (*G*, *Left*) Pulmonary metastasis in WT and *Vegfr1 tk*$^{-/-}$ mice bearing vector- and VEGF-B-T241 tumors. Arrowheads indicate metastatic nodules. Dashed lines encircle metastatic nodules. [Scale bar, 5 mm (*Top*); 100 μm (*Middle* and *Bottom*).] (*Right*) The bar chart shows the percentage of mice with visible lung metastases (n = 10–11 animals per group). All error bars represent SEM. All P values were analyzed according to Student's t test. ns, not significant. (*H*) Kaplan–Meier survival curves of *VEGFB* high-expressing (n = 214) and *VEGFB* low- expressing (n = 197) LSCC cancer patients (*Left*) and *VEGFB* high-expressing (n = 197) and *VEGFB* low-expressing (n = 218) melanoma cancer patients (*Right*).

average level were considered the low-expression group. In a large cohort of 411 human patients with lung squamous cell carcinoma (LSCC), the 214 patients with high *VEGFB* expression in their tumors had significantly shortened survival than the 197 patients with low *VEGFB* expression levels (Fig. 6*H*). Similarly, in a large cohort study of 415 melanoma patients, the 197 patients with high *VEGFB* expression exhibited significantly poorer survival than the 218 patients with low *VEGFB* expression (Fig. 6*H*). These clinical data support our preclinical studies and suggest that VEGF-B–promoted cancer metastasis is likely to be the mechanism for poor survival in human cancer patients.

Discussion

The metastatic cascade is a complex multistep process that involves intimate and corporative interactions between malignant cells and host cells at the primary sites as well as in distal tissues. At the primary tumor site, tumor invasion and metastasis are initiated at the early stage of tumor development by both the intrinsic genetic features of malignant cells and alterations in the tumor microenvironment (31). Increasing evidence shows that alterations of the tumor microenvironment, including microvessels, hypoxia, and infiltration and activation of inflammatory cells and the stromal fibroblasts, play a predominant role in facilitating cancer metastasis

(7). To be disseminated to distal tissues and organs, tumor cells must intravasate through the vessel wall into the circulation. Intravasation probably is the most crucial step of the entire metastatic cascade, and microvessels are the structural barriers that prevent tumor cell invasion. Tumor cells often produce signaling molecules that manipulate microvessels and other host-derived cellular components to become highly permissive for their invasion. Our present work provides another example of how tumor cells, by producing VEGF-B, propagate the structures of microvessels for invasion and metastasis.

Our data provide a previously unidentified mechanism of cancer metastasis that occurs along with the reduction of primary tumor growth and thus uncouples metastasis from primary tumor growth. Unlike most other angiogenic factors, including VEGF-A, VEGF-C, FGF-2, PDGF-BB, and angiopoietins, VEGF-B does not stimulate tumor angiogenesis in our experimental settings. Rather, it markedly modulates vascular structures with decreased perivascular cell coverage and increased leakiness, leading to a reduced rate of tumor growth. One of the most striking findings is that VEGF-B induces normalization of tumor vasculatures that are highly leaky. Paradoxically, anti–VEGF-A drugs such as bevacizumab also have been claimed to induce normalized vasculatures with reduced vascular permeability (28, 32). Although VEGF-B–modulated and anti–VEGF-A drug-modulated tumor vessels exhibit a similar phenotype, lacking excessive sprouting and branches, they display opposing effects of perivascular coverage and vascular permeability. Placental growth factor (PlGF), another member of the VEGF family closely related to VEGF-B, also remodels tumor vasculature toward a normalized phenotype through a VEGF-A–dependent mechanism of spatiotemporal vascular regulation (28, 29). In contrast to VEGF-B, PlGF-normalized tumor vasculatures are highly dilated, are tightly coated with perivascular cells, and are not permeable. Interestingly, both PlGF and VEGF-B bind to VEGFR1, but they display opposing effects in remodeling tumor vessels. At the time of this writing, the molecular mechanisms that underlie the functional differences between VEGF-B and PlGF are unknown.

One of the main differences between VEGF-B and the anti–VEGF-A drug bevacizumab is that the former is a functional growth factor, whereas the latter blocks VEGF function exclusively. It is reasonable to speculate that VEGF-B, in addition to modulating VEGF-A–mediated vascular functions, might display other functions through interactions with its receptors. Activation of VEGFR1 by VEGF-B potentially could remodel tumor vasculatures that facilitate cancer metastasis. Surprisingly, deletion of the tyrosine kinase domain of VEGFR1 in mice does not affect VEGF-B–induced vascular remodeling and metastasis, suggesting the existence of a VEGFR1-independent mechanism of metastasis. This finding raises an important question about the receptor type that mediates VEGF-B–induced vascular remodeling and metastasis. Through which receptor does VEGF-B promote cancer metastasis? Would neuropilin1 (NRP1) be a potential receptor for these effects? If so, why do other NRP1-binding ligands such as PlGF not produce vascular remodeling and metastatic effects similar to those of VEGF-B? VEGF-B and PlGF are the two most structurally and functionally closely related ligands within the VEGF family (16). Both growth factors bind VEGFR1 exclusively, lack the ability to induce angiogenesis, and negatively regulate tumor angiogenesis. However, our own and others' work shows that PlGF expression in tumors does not seem to confer an invasive phenotype (28, 33–35), although tumor-promoting effects of PlGF also have been described (36). The functional differences in the vascular remodeling and cancer invasion effects of VEGF-B and PlGF suggest that VEGF-B might bind to another, as yet unidentified receptor that lacks interaction with PlGF. This possibility warrants further investigation.

The mechanism by which VEGF-B promotes cancer metastasis is likely to occur at the intravasation process because animals bearing VEGF-B tumors have high numbers of CTCs. Several vasculature-related parameters support VEGF-B–induced cancer cell intravasation: (*i*) ablation of perivascular cells from tumor vasculatures; (*ii*) increased vascular leakage; (*iii*) tissue hypoxia; and (*iv*) recruitment of inflammatory macrophages in tumors (Fig. 7). The ablation of perivascular cells and high vascular permeability would increase the possibility of tumor cell intravasation. TAMs are known to guide tumor cells into the circulation for intravasation and thus increase CTCs (8). Moreover, inflammatory cells also might promote the formation of the initial metastatic niches in distal tissues and organs. Tumor hypoxia potentially could encourage tumor cells to invade neighboring healthy tissues for the uptake of nutrition and oxygen, leading to an invasive phenotype. Hypoxia also is a potent inducer of the elevated expression of an array of growth factors and cytokines such as VEGF-A (37–40), which in turn increase vascular leakage and vascular tortuosity. Our present findings demonstrate that it is unlikely that VEGF-A plays a critical role in mediating VEGF-B–promoted cancer metastasis, because the genetic deletion of VEGF-A in tumor cells and the pharmacological inhibition of VEGF-A do not affect VEGF-B–induced metastasis significantly. Although modulation of VEGF-A–induced angiogenesis and vascular permeability by VEGF-B inevitably would occur because of the potential formation of the VEGF-B-/VEGF-A heterodimers, as previously described, VEGF-B on its own certainly would elicit additional functions that are independent of VEGF-A. Interestingly, the role of VEGF-B in ablating pericytes and increasing vascular leakage in tumor vessels resembles a scenario in which Angiopoietin-2 increases vascular permeability by repelling pericytes, possibly by increasing the production of superoxide (41–43).

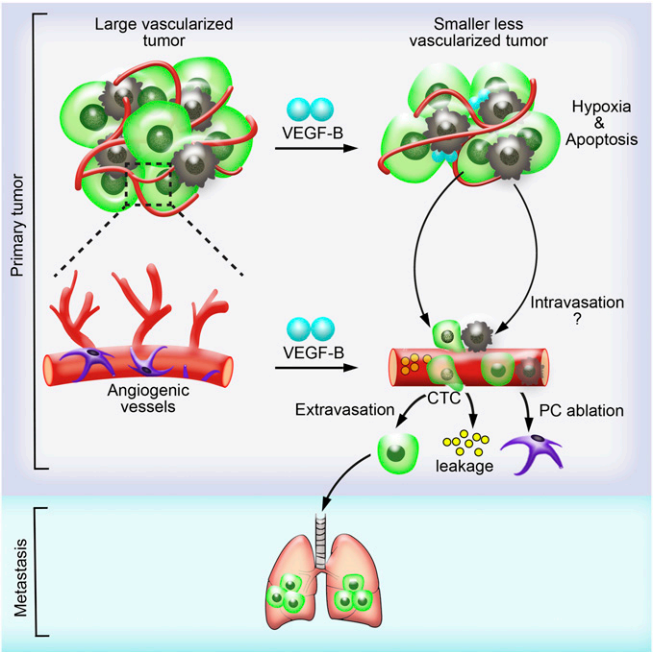

Fig. 7. Schematic illustration of VEGF-B–induced tumor vessel remodeling and metastasis. The tumor-derived high VEGF-B level leads to the suppression of tumor angiogenesis and increased cell death. As a consequence, primary tumor growth is impaired, and the tumor microenvironment becomes more hypoxic. However, VEGF-B facilitates tumor cell intravasation by generating highly leaky vasculature in tumor and recruiting M2-like macrophages, thus giving rise to more severe pulmonary metastasis.

In two large cohort studies of human cancer patients with nontreated LSCC and melanoma, VEGF-B expression levels were reversely correlated with survival. In these cancer types, it is known that cancer invasion and metastasis are the most common cause of death. Thus, it is reasonable to speculate that the mechanism that underlies VEGF-B–related mortality is related to cancer metastasis. In this regard, VEGF-B expression in these cancers, and perhaps in other cancer types, could serve as a predictive marker for cancer patients' survival. However, various treatment regiments are likely to affect VEGF-B expression levels, and the predictive value of this single marker for patient survival remains a challenging issue.

Materials and Methods

Animals, Mouse Tumor Model, Zebrafish Tumor Dissemination Model, and Clinical Data Analysis. All animal studies were approved by the North Stockholm Experimental Animal Ethical Committee. Mouse tumor model: Cultured tumor cells were suspended at the concentration of 1×10^7/mL or 1×10^6 cells in 100 μL of PBS and were subcutaneously injected into the dorsal back of each mouse. Zebrafish model: Zebrafish embryos were dechorionated at 48 hpf and anesthetized with 0.04 mg/mL of tricaine. Approximately, 300–500 tumor cells labeled with DiI die were resuspended in serum-free DMEM, followed by injection into the perivitelline space of each embryo. Clinical data was from TCGA and was analyzed using Kaplan–Meier survival method followed by log-rank test. Details are provided in *SI Materials and Methods*.

Tissue Hypoxia Analysis, Vascular Perfusion, and Permeability Assay. Hypoxia in tumor tissues was detected according to a standard protocol using the Hypoxyprobe HP2-1000 kit. Dextran 2000-kDa or 70-kDa were used for vascular perfusion and permeability assay. See *SI Materials and Methods* for details.

Histological Studies, Immunohistochemistry, Immunofluorescent Staining, and Whole-Mount Staining. Standard protocol were applied. See *SI Materials and Methods* for details.

In Vitro Studies, Including FACS Analysis, Western Blotting, ELISA, VEGF-B Overexpression, shRNA, and Quantitative PCR. See *SI Materials and Methods* for details of in vitro studies.

ACKNOWLEDGMENTS. We thank Dr. Masabumi Shibuya at Tokyo University for providing the *Vegfr1 tk*$^{-/-}$ mice and Dr. Janusz Rak at the McGill University Health Center for providing the 528ras cells. The Y.C. laboratory is supported by research grants from the Swedish Research Council, the Swedish Cancer Foundation, the Karolinska Institute Foundation, the Torsten Soderberg Foundation, European Research Council Advanced Grant ANGIOFAT (Project 250021), and a Novo Nordisk Foundation advanced grant. Y.C. is the recipient of a Karolinska Institute distinguished professor award.

1. Hanahan D, Weinberg RA (2011) Hallmarks of cancer: The next generation. *Cell* 144(5):646–674.
2. Folkman J (1971) Tumor angiogenesis: Therapeutic implications. *N Engl J Med* 285(21):1182–1186.
3. Cao Y, et al. (2011) Forty-year journey of angiogenesis translational research. *Sci Transl Med* 3(114):114rv3.
4. Cao Y, Langer R (2010) Optimizing the delivery of cancer drugs that block angiogenesis. *Sci Transl Med* 2(15):ps3.
5. Hurwitz H, et al. (2004) Bevacizumab plus irinotecan, fluorouracil, and leucovorin for metastatic colorectal cancer. *N Engl J Med* 350(23):2335–2342.
6. Lees CW, Ironside J, Wallace WA, Satsangi J (2008) Resolution of non-small-cell lung cancer after withdrawal of anti-TNF therapy. *N Engl J Med* 359(3):320–321.
7. Joyce JA, Pollard JW (2009) Microenvironmental regulation of metastasis. *Nat Rev Cancer* 9(4):239–252.
8. Pollard JW (2004) Tumour-educated macrophages promote tumour progression and metastasis. *Nat Rev Cancer* 4(1):71–78.
9. Psaila B, Lyden D (2009) The metastatic niche: Adapting the foreign soil. *Nat Rev Cancer* 9(4):285–293.
10. Gupta GP, Massagué J (2006) Cancer metastasis: Building a framework. *Cell* 127(4): 679–695.
11. Jubb AM, et al. (2004) Expression of vascular endothelial growth factor, hypoxia inducible factor 1alpha, and carbonic anhydrase IX in human tumours. *J Clin Pathol* 57(5):504–512.
12. Cao Y, Liu Q (2007) Therapeutic targets of multiple angiogenic factors for the treatment of cancer and metastasis. *Adv Cancer Res* 97:203–224.
13. Kim KJ, et al. (1993) Inhibition of vascular endothelial growth factor-induced angiogenesis suppresses tumour growth in vivo. *Nature* 362(6423):841–844.
14. Senger DR, et al. (1983) Tumor cells secrete a vascular permeability factor that promotes accumulation of ascites fluid. *Science* 219(4587):983–985.
15. Sawamiphak S, et al. (2010) Ephrin-B2 regulates VEGFR2 function in developmental and tumour angiogenesis. *Nature* 465(7297):487–491.
16. Cao Y (2009) Positive and negative modulation of angiogenesis by VEGFR1 ligands. *Sci Signal* 2(59):re1.
17. Shibuya M (2006) Vascular endothelial growth factor receptor-1 (VEGFR-1/Flt-1): A dual regulator for angiogenesis. *Angiogenesis* 9(4):225–230, discussion 231.
18. Olofsson B, et al. (1996) Vascular endothelial growth factor B, a novel growth factor for endothelial cells. *Proc Natl Acad Sci USA* 93(6):2576–2581.
19. Li X, et al. (2009) VEGF-B: A survival, or an angiogenic factor? *Cell Adhes Migr* 3(4): 322–327.
20. Albrecht I, et al. (2010) Suppressive effects of vascular endothelial growth factor-B on tumor growth in a mouse model of pancreatic neuroendocrine tumorigenesis. *PLoS ONE* 5(11):e14109.
21. Zhang F, et al. (2009) VEGF-B is dispensable for blood vessel growth but critical for their survival, and VEGF-B targeting inhibits pathological angiogenesis. *Proc Natl Acad Sci USA* 106(15):6152–6157.
22. Rouhi P, et al. (2010) Hypoxia-induced metastasis model in embryonic zebrafish. *Nat Protoc* 5(12):1911–1918.
23. Lee SL, et al. (2009) Hypoxia-induced pathological angiogenesis mediates tumor cell dissemination, invasion, and metastasis in a zebrafish tumor model. *Proc Natl Acad Sci USA* 106(46):19485–19490.
24. Dahl Ejby Jensen L, et al. (2009) Nitric oxide permits hypoxia-induced lymphatic perfusion by controlling arterial-lymphatic conduits in zebrafish and glass catfish. *Proc Natl Acad Sci USA* 106(43):18408–18413.
25. Lawson ND, Weinstein BM (2002) In vivo imaging of embryonic vascular development using transgenic zebrafish. *Dev Biol* 248(2):307–318.
26. Viloria-Petit A, et al. (2003) Contrasting effects of VEGF gene disruption in embryonic stem cell-derived versus oncogene-induced tumors. *EMBO J* 22(16):4091–4102.
27. Yang Y, et al. (2013) Anti-VEGF- and anti-VEGF receptor-induced vascular alteration in mouse healthy tissues. *Proc Natl Acad Sci USA* 110(29):12018–12023.
28. Hedlund EM, et al. (2013) Tumor cell-derived placental growth factor sensitizes antiangiogenic and antitumor effects of anti-VEGF drugs. *Proc Natl Acad Sci USA* 110(2): 654–659.
29. Yang X, et al. (2013) Vascular endothelial growth factor-dependent spatiotemporal dual roles of placental growth factor in modulation of angiogenesis and tumor growth. *Proc Natl Acad Sci USA* 110(34):13932–13937.
30. Hiratsuka S, Minowa O, Kuno J, Noda T, Shibuya M (1998) Flt-1 lacking the tyrosine kinase domain is sufficient for normal development and angiogenesis in mice. *Proc Natl Acad Sci USA* 95(16):9349–9354.
31. Rouhi P, et al. (2010) Pathological angiogenesis facilitates tumor cell dissemination and metastasis. *Cell Cycle* 9(5):913–917.
32. Jain RK (2005) Normalization of tumor vasculature: An emerging concept in antiangiogenic therapy. *Science* 307(5706):58–62.
33. Schomber T, et al. (2007) Placental growth factor-1 attenuates vascular endothelial growth factor-A-dependent tumor angiogenesis during beta cell carcinogenesis. *Cancer Res* 67(22):10840–10848.
34. Xu L, et al. (2006) Placenta growth factor overexpression inhibits tumor growth, angiogenesis, and metastasis by depleting vascular endothelial growth factor homodimers in orthotopic mouse models. *Cancer Res* 66(8):3971–3977.
35. Eriksson A, et al. (2002) Placenta growth factor-1 antagonizes VEGF-induced angiogenesis and tumor growth by the formation of functionally inactive PlGF-1/VEGF heterodimers. *Cancer Cell* 1(1):99–108.
36. Fischer C, et al. (2007) Anti-PlGF inhibits growth of VEGF(R)-inhibitor-resistant tumors without affecting healthy vessels. *Cell* 131(3):463–475.
37. Makino Y, et al. (2001) Inhibitory PAS domain protein is a negative regulator of hypoxia-inducible gene expression. *Nature* 414(6863):550–554.
38. Mandriota SJ, et al. (2002) HIF activation identifies early lesions in VHL kidneys: Evidence for site-specific tumor suppressor function in the nephron. *Cancer Cell* 1(5): 459–468.
39. Millauer B, Shawver LK, Plate KH, Risau W, Ullrich A (1994) Glioblastoma growth inhibited in vivo by a dominant-negative Flk-1 mutant. *Nature* 367(6463):576–579.
40. Shweiki D, Itin A, Soffer D, Keshet E (1992) Vascular endothelial growth factor induced by hypoxia may mediate hypoxia-initiated angiogenesis. *Nature* 359(6398): 843–845.
41. Arbiser JL, Bips M, Seidler A, Bonner MY, Kovach C (2012) Combination therapy of imiquimod and gentian violet for cutaneous melanoma metastases. *J Am Acad Dermatol* 67(2):e81–e83.
42. Bonner MY, Arbiser JL (2014) The antioxidant paradox: What are antioxidants and how should they be used in a therapeutic context for cancer. *Future Med Chem* 6(12): 1413–1422.
43. Munson JM, et al. (2012) Anti-invasive adjuvant therapy with imipramine blue enhances chemotherapeutic efficacy against glioma. *Sci Transl Med* 4(127):127ra36.